INTERNATIONAL JOURNAL OF AUTOMOTIVE AND MECHANICAL ENGINEERING (IJAME)
ISSN: 2229-8649 e-ISSN: 2180-1606
VOL. 17, ISSUE 2, 7816 – 7831
DOI: https://doi.org/10.15282/ijame.17.2.2020.01.0582

ORIGINAL ARTICLE

Experimental Analysis on the Transduction Coefficient of a Non-Linear Electromagnetic Energy Harvesting Device with Softening Stiffness

P. S. Low, R. Ramlan* , H. A. Ghani and N. S. Muhammad

Centre for Advanced Research on Energy, Faculty of Mechanical Engineering, Universiti Teknikal Malaysia Melaka, Hang Tuah Jaya, 76100 Durian Tunggal, Melaka, Malaysia
Phone: +6062704367; Fax: +606-2701046

ABSTRACT – Non-linear energy harvesting devices in the form of stiffness non-linearity have emerged as among the effective solutions to overcome the performance limit of linear energy harvesting devices. However, up to now, researches on the non-linear devices are only focusing on the ability to widen the bandwidth while the limit of employing linear transduction coefficient in a non-linear system has yet to be heavily discussed. This paper investigates on the transduction coefficient for both linear and non-linear systems of an electromagnetic energy harvesting device as a function of the excitation frequency. It is proven that the transduction coefficient of the non-linear device is larger than its equivalent linear device, especially in the multi-stable solutions region. In common practice, the non-linearity in the non-linear system is considered weak, and its transduction coefficient is assumed to converge to the one produced by the linear system. The limits to which the transduction coefficient of a linear system can be employed on the non-linear system were drawn based on the experimental analysis conducted on the proposed device. The device was designed to perform as a linear or non-linear system, where the degree of non-linearity was changed by varying the gap between the magnets. The limit of the transduction coefficient was determined from the analysis of the harmonic ratio. The results show that the linear transduction coefficient is valid to be employed to the non-linear system when the harmonic ratio is less than five per cent at the multi-stable solutions region.

ARTICLE HISTORY
Revised:23rd Apr 2020
Accepted: 29th June 2020

KEYWORDS
Transduction coefficient, Energy harvesting, Non-linear softening, Duffing.

INTRODUCTION

In the early days, the linear resonant vibration-based energy harvesting device has been the pioneer of the energy harvesting operating principle. It works by tuning the natural frequency of the device to match the ambient frequency. This single tuning frequency operating principle gives limitation to the existing linear device, especially when dealing with applications of varying frequency. Another possible limitation of the harvester is the maximum amount of power it can generate for specific applications since the power is proportional to the relative displacement. Large relative displacement is often limited by the size of the housing.

Non-linear vibration-based energy harvesting devices have been the popular choice in the field to improve the performance limit of the linear resonant generator. Among many types of non-linearities that can be introduced into the system, stiffness non-linearity is one of them. The dynamics of the system with stiffness non-linearity can be characterised by using Duffing's equation in which the total stiffness comprises of both linear and non-linear stiffness coefficients. Currently, the focus of the benefit of having non-linear stiffness in the mechanism of an energy harvesting device is mainly on bandwidth widening [1-3]. The amount of power that can be generated is often considered less significant as long as the device can provide better bandwidth. A few well-known factors that may affect the power generation include frequency, relative displacement, amount of damping and transduction coefficient. The last factor often receives less attention in the non-linear energy harvesting device.

Permanent magnet based electromagnetic energy harvester is one of the electromechanical coupling methods to generate electrical energy resulting from mechanical motion. This method has been widely used to power application in terms of micro rather than macro applications for the last decade [6-13]. It works based on Faraday's law, where the relative motion between magnet and coil produces voltage [14]. The energy conversion performance of these harvesters relies on the relation between the mechanical domain and the electrical domain. This electromechanical relation is typically described using the expression $K = NlB$ where K is referred as the transduction coefficient, N is the number of coil turns, l is the length of the coil and B is the magnetic flux density across the coil. The performance of K can be improved by either increasing the number of coil turns or the length of the coil or by using a magnet with high residual flux density. However, it is worth to note that modelling and optimising the transduction coefficient K is not the aim of this paper. This paper highlights the potential of having larger transduction coefficient as an added benefit of non-linear energy harvesting devices in addition to the commonly claimed bandwidth widening capability.

*CORRESPONDING AUTHOR | R. Ramlan | ✉ roszaidi@utem.edu.my

The majority of prior research has addressed the 'transduction coefficient' term in many ways. Some of them addressed the term as 'electromagnetic coupling coefficient' [15], 'electromechanical coupling coefficient' [16], 'electromagnetic coupling factor' [7, 17] and 'electromagnetic coupling' [18]. Regardless of the variation of the terms, K brings similar intention, which is to describe the relationship between the mechanical and electrical domains of the electromagnetic energy harvester having units of Vsm^{-1} or NA^{-1} [19]. The transduction coefficient can be quantified as the voltage generated, V per unit of relative velocity, v or the mechanical force, F generated per unit of electric current, i.

There exists a considerable number of literature with regards to the determination of the transduction coefficient, K on the linear system of the electromagnetic energy harvester [7, 20-21]. In the study, the transduction coefficient was determined by giving a known value of direct current (DC), and the corresponding deflection of the seismic mass was measured. The deflection of the seismic mass is proportional to the generated restoring force in the cantilever beam. The transduction coefficient was then determined by taking the ratio between the force and the supplied DC. As for the non-linear system, far too little attention has been paid in determining or examining the effect of transduction coefficient on its performance. Although the transduction coefficient, K has been mentioned by [16, 22] in their derivation to obtain maximum power for non-linear electromagnetic energy harvester, specific analysis to determine K for the non-linear system has yet to be established.

Up to now, there is very little study investigating the transduction coefficient of the non-linear energy harvesting device. In particular, transduction characteristics for non-linear energy harvesting device, specifically the softening system and the effect of the non-linearity on the transduction coefficient as a function of excitation frequency have yet to be explored in the scientific literature. A much-debated question about the transduction coefficient of the electromagnetic energy harvesting device lies between the unclear impacts of using the linear transduction coefficient on the non-linear system. The research to date has tended to focus on the linear transduction coefficient rather than the non-linear as the non-linear system is considered to be weak and the characteristic was assumed to converge to the linear system.

This paper determines the transduction coefficient for both linear and non-linear system across a range of excitation frequency. The effect of the non-linearity on the transduction coefficient, specifically in the multi-stable frequency range will be focused on. In addition, this paper also aims to highlight the limit to which the linear transduction coefficient can be employed on the non-linear system of an electromagnetic energy harvesting device. This study uses the experimental analysis approach to examine the transduction coefficient of an electromagnetic energy harvester for respective linear and non-linear system.

In this paper, the effect of the degree of non-linearity on the transduction coefficient for both linear and non-linear system was addressed. The next section introduces the transduction coefficient in the linear and non-linear systems. Section two elaborates the design of the proposed electromagnetic energy harvesting device. The section continues with the derivation of the average power generated from the base-excited energy harvesting device with the influence of transduction coefficient. In the fifth section, the method and setup of the experimental investigation are elaborated. A series of processed experimental results obtained from the experiments are analysed and presented. The last section summarises the findings and insights realised from this study.

DESIGN OF THE ENERGY HARVESTING DEVICE

The energy harvesting device in this study is presented in Figure 1 and 2. The architecture of the device can be divided into two parts. The first controls the degree on linearity using a steel beam which is fixed at one end and free at the other end. The free end is attached with a tungsten mass. A magnet is attached at the tip mass in the direction perpendicular to the axis of oscillation. The device is designed with an adjustable slider with two attached magnets which repulse the magnet on the tungsten tip mass, as shown in Figure 2(b). This adjustable slider is used to vary the gap between the magnets, d. When the gap is small, the overall stiffness results from the combination of both linear stiffness from the beam and the non-linear magnetic stiffness from the repulsive magnetic force. When the gap gets larger, the contribution from the non-linear magnetic stiffness weakens, hence reducing the degree of non-linearity of the system. The adjustable slider can even be removed completely to represent a linear system.

The second part of the device is for voltage generation, which consists of a stationary copper coil and a magnet attached to the side of the tungsten mass. This magnet has no influence in altering the overall stiffness of the system. The side magnets change the magnetic flux across the stationary copper coil during oscillation, hence producing voltage. The parameters for the proposed device are presented in Table 1.

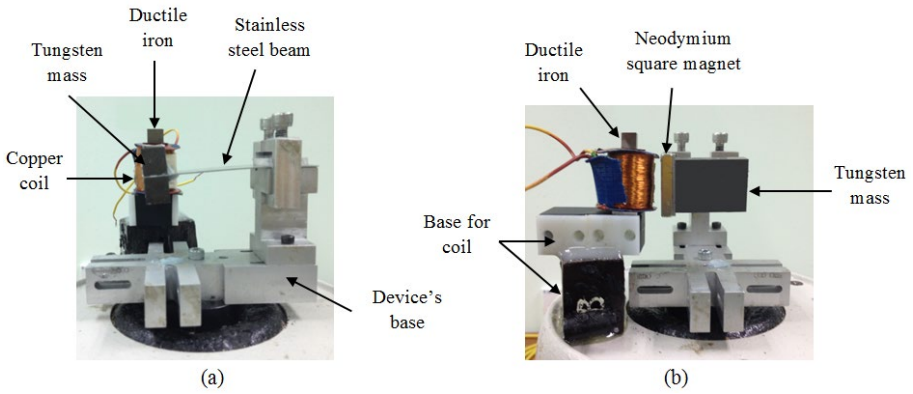

Figure 1. (a) Front view and (b) side view of the linear configuration for the electromagnetic energy harvesting device.

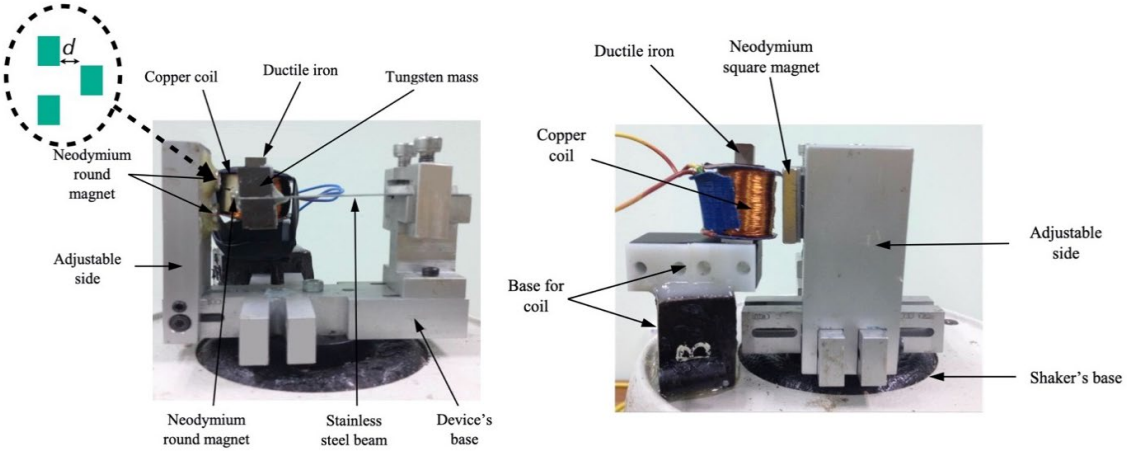

Figure 2. (a) Front view and (b) side view of the non-linear configuration for the electromagnetic energy harvesting device. The inset in (a) shows the magnet configuration where d is the gap between magnets.

Table 1. List of fixed parameters for the proposed device.

Parameter	Dimensions (mm)	Descriptions
Copper coil	φ 0.1	3500 turns, R_{int} = 223 ± 0.1 Ohm
Round magnet	φ 8.0	Neodymium, 1.7 kg pull force
Square magnet	25 (l) × 10 (w) × 5 (t)	Neodymium, 4.9 kg pull force
Beam	50 (l) × 30 (w) × 0.5 (t)	Stainless steel

RELATION OF POWER WITH TRANSDUCTION COEFFICIENT

The energy harvesting device is modelled as a base excited mass-spring-damper system, as shown in Figure 3(a). The equation of motion for the non-linear system can be written as:

$$m\ddot{z} + c\dot{z} + k_1 z - k_3 z^3 = -m\ddot{y} \tag{1}$$

where c is the total damping coefficient comprises of both the mechanical c_m and electrical damping c_e and $z = x - y$ is the relative displacement between the seismic mass, x and input excitation, $y = Y\cos(\omega t)$, and ω is the excitation frequency. Notice the stiffness comprises of both linear stiffness, k_1 and non-linear stiffness, k_3. The negative sign before k_3 indicates the non-linear softening stiffness. The equation can be further expressed in non-dimensional form as:

$$u'' + 2\zeta u' + u - \alpha u^3 = \Omega^2 \cos(\Omega\tau + \phi) \tag{2}$$

where $(u)' = \frac{d}{d\tau}$, $(u)'' = \frac{d^2}{d\tau^2}$, $u = \frac{z}{Y}$, $2\zeta = \frac{c}{m\omega_n}$, $\omega_n^2 = \frac{k_1}{m}$, $\alpha = \frac{k_3}{k_1}Y^2$, $\Omega = \frac{\omega}{\omega_n}$, $\tau = \omega_n t$ is the non-dimensional time, ω_n is the undamped natural frequency, and ϕ is the phase angle between excitation and response. Subsequently, Eq. (2) is solved using the harmonic balance method to obtain the frequency-amplitude relation of the non-linear system by assuming that the response is dominated by the fundamental frequency, i.e. $u = U\cos(\Omega\tau)$. It is worth to note here that this paper does not intend to focus on the detailed analytical modelling of the dynamics of the system. For a detail analytical study on the dynamics of the system, readers are referred to Ramlan et al. [23]. The frequency-amplitude relation of the system is given by:

$$\Omega = \sqrt{\frac{4U^2 1 - 2\zeta^2 - 3\alpha U^4 \pm U\sqrt{(3\alpha U^2 - 4)^2 + 64U^2\zeta^2 - 1 + 48U^4\zeta^2\alpha}}{4(U^2 - 1)}} \tag{3}$$

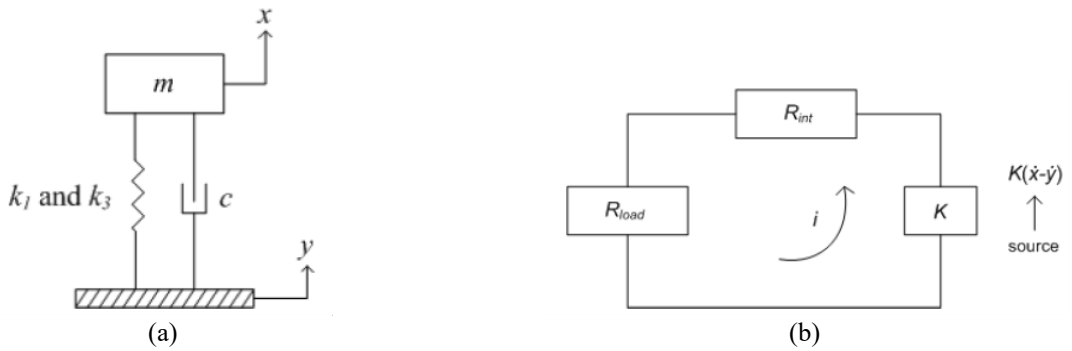

Figure 3. (a) Mass-spring-damper model of an energy harvesting device with stiffness non-linearity and (b) electrical equivalent circuit diagram for an energy harvesting device

Figure 4 shows a typical frequency response curve for a non-linear softening stiffness system plotted using Eq. (3). The resonant branch is obtained by sweeping down the excitation frequency. The response follows IV-III-V route. Point V gives the maximum values of the response $U_{\max}$ which occurs at the jump-down frequency Ω_{down}. A slight decrease in the frequency causes a sudden jump of the response down to the non-resonant branch with a smaller amplitude and follows route VI-I. The non-resonant branch is obtained by sweeping up the excitation frequency. The response on the branch follows I-VI-II route. A slight increase in the frequency causes a sudden jump of the response to location III, which is referred to as the jump-up point. Further increase in the frequency causes the system to respond on the mono-stable resonant branch from III to IV.

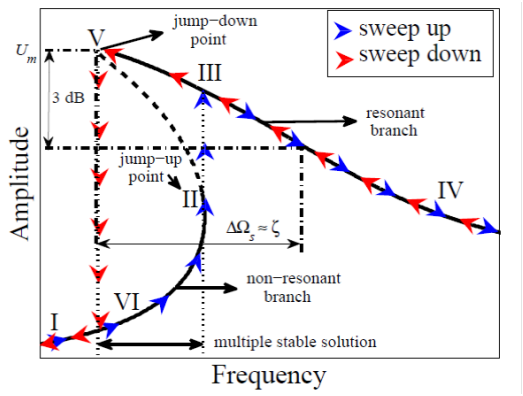

Figure 4. The typical frequency response curve for the non-linear softening system.

The maximum response, $U_{\max}$ and the jump-down frequency, Ω_{down} are respectively given by [23].

$$U_{\max} = \frac{1}{2\zeta}\sqrt{\frac{1}{1 + \frac{3\alpha}{16\zeta^2}}} \tag{4}$$

$$\Omega_{\text{down}} = \sqrt{\frac{1}{1 + \frac{3\alpha}{16\zeta^2}}} \tag{5}$$

The electrical equivalent of the proposed electromagnetic energy harvesting device is shown in Figure 3(b). Applying Kirchhoff's voltage law to the equivalent electrical circuit diagram results in the following equation

$$i(R_{\text{load}} + R_{\text{int}}) - K(\dot{x} - \dot{y}) = 0 \tag{6}$$

where K is the transduction coefficient, i is the induced electrical current, R_{load} is the load resistance and R_{int} is the internal resistance of the coil. The expression for the electrical current, i is obtained by rearranging Eq. (6) to yield

$$i = \frac{K(\dot{x} - \dot{y})}{R_{\text{load}} + R_{\text{int}}} \tag{7}$$

The instantaneous power, P_{inst} transferred to the electrical load, R_{load} is expressed as:

$$P_{inst} = i^2 R_{load} \tag{8}$$

In the modelling of the proposed device discussed earlier, the electrical current, i, is shown in Eq. (7). Since the device in this study is subjected to harmonic excitation, the expression of $\dot{x} - \dot{y}$ can be replaced by its non-dimensional form of $\dot{u} = -\Omega U \sin(\Omega\tau)$ to yield:

$$i = -\frac{K}{R_{\text{load}} + R_{\text{int}}} \Omega U \sin(\Omega\tau - \phi) \tag{9}$$

By substituting Eq. (9) into Eq. (8), P_{inst} becomes

$$P_{\text{inst}} = \frac{1}{2}\left(\frac{K\Omega U}{R_{\text{load}} + R_{\text{int}}}\right)^2 R_{\text{load}}[1 - \cos 2(\Omega\tau - \phi)] \tag{10}$$

The time-averaged power to the electrical load P_{avg} is now given by [24]

$$P_{\text{avg}} = \frac{1}{2}\left(\frac{K\Omega U}{R_{\text{load}} + R_{\text{int}}}\right)^2 R_{\text{load}} \tag{11}$$

The maximum time-averaged power of a non-linear softening system occurs at the jump-down point. By substituting the amplitude of the maximum response, U_{max} and the jump-down frequency, Ω_{down} into Eq. (11), the maximum time-averaged power is now given by

$$P_{\text{avg}} = \frac{1}{2}\left(\frac{K\Omega_{\text{down}} U_{\text{max}}}{R_{\text{load}} + R_{\text{int}}}\right)^2 R_{\text{load}} \tag{12}$$

Equation (12) shows that the maximum time-averaged power to the electrical load depends not only on the maximum response and jump-down frequency but also on the transduction coefficient. Unlike the non-linear hardening system, where the frequency response curve bends to the right which results in high jump-down frequency as reported in [23], the frequency response curve of the softening system bends to the left as shown in Figure 4. The highly non-linear softening system tends to lower the jump-down frequency.

Figure 5 shows the effect of both Ω_{down} and U_{max} on the power harvested by a non-linear softening system. The trend of the power curve is represented by the product of both parameters. It should be noted that the power harvested by the non-linear softening system is always less than its equivalent linear system which is indicated by $\alpha^2/\zeta \to 0$. However, the maximum power generation is not always the main objective of a non-linear system. As for the non-linear softening system, the aim is more towards tapping the wideband low-frequency energy. This can be achieved by increasing the degree of non-linearity. An increase in the degree of non-linearity lowers the Ω_{down} and U_{max}. This, in effects, reduces the amount of power to be harvested. From Eq. (12), a large transduction coefficient could compensate for, to a certain degree, the effect caused by the low jump-down frequency and maximum response.

EXPERIMENTAL METHOD AND SETUP

In this study, two types of experimental measurement were demonstrated on the linear and non-linear configurations of the energy harvesting device in order to study the frequency response characteristic and to determine the transduction coefficient. The degree of non-linearity for the non-linear configuration was determined using quasi-static measurement results. Next is the dynamic measurement where the dynamic characteristics were examined, and the transduction coefficient for linear and non-linear configurations was evaluated.

Quasi-Static Measurement

Figure 6 illustrates the experimental setup for the quasi-static measurement. This experimental method was conducted with the purpose of analysing the restoring force-deflection characteristic and estimating the non-linearity of the proposed electromagnetic energy harvesting device. The non-linearity is useful when it comes to determining the limit of employing linear transduction in a non-linear system.

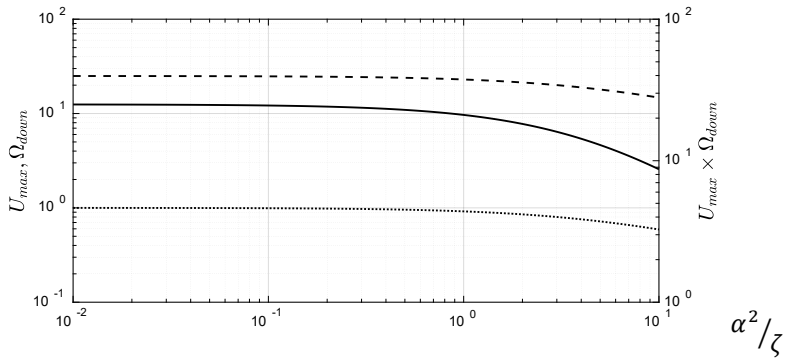

Figure 5. Variation of the jump-down frequency, $\boldsymbol{\Omega_{down}}$ (···), the maximum response, $\boldsymbol{U_{max}}$ (---) and $\boldsymbol{U_{max} \times \Omega_{down}}$ (−) with respect to $\boldsymbol{\alpha^2/\zeta}$ with $\boldsymbol{\zeta = 0.02}$.

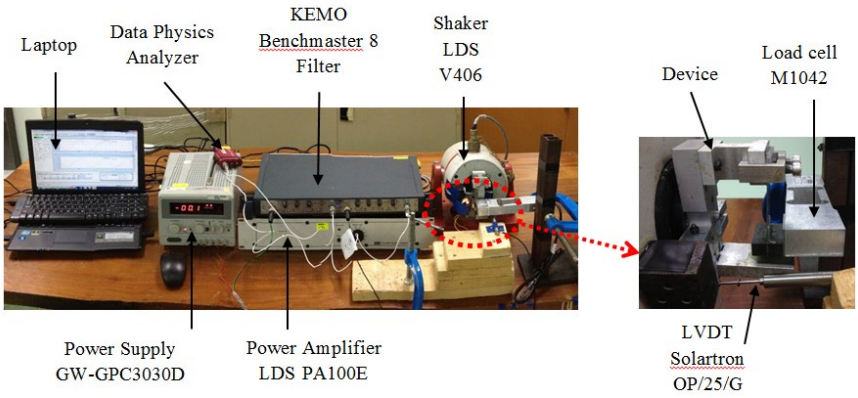

Figure 6. Experimental setup for quasi-static measurement.

In the experiment setup, the device was placed on the LDS V406 shaker with the shaker being tilted horizontally to reduce asymmetries from the effect of gravity towards the beam during measurement as practised in [25]. A Huntleigh M1042 beam type load cell was attached directly on the tungsten mass's surface while the Solartron OP/25/G linear variable differential transformer (LVDT) was firmly attached to the base of the proposed device. Both the load cell and LVDT were powered by a constant 10V DC from the GW-GPC3030D power supply. The outputs from the respective load cell and LVDT were filtered by KEMO Benchmaster 8 Filter and then analysed by the Data Physics Quattro dynamic signal analyser.

Dynamic Measurement

The schematic diagram for the dynamic measurement arrangement is presented in Figure 7. This measurement was performed in order to obtain the frequency response curve and the transduction coefficient. The frequency response curve of the device is an important aspect to be studied especially due to the existence of the multi-stable solutions region in the non-linear system.

In the course of the experiment, the energy harvesting device was securely tightened to the base of LDS V406 shaker vertically. Two Dytran accelerometers were respectively mounted to the top surface of tungsten mass and the device's base. Both accelerometers were connected to the Data Physics Quattro dynamic signal analyser to record the response of the device when being excited with constant amplitude harmonic excitation. The accelerometer on the tungsten mass was used to obtain the response of the beam when the device was swept-up (10 Hz to 40 Hz) and swept-down (40 Hz to 10 Hz) with a step size of 1 Hz at constant amplitude input displacement of 1 mm under open circuit condition. The accelerometer on the base of the device maintained the amplitude of excitation through the gain adjustment of the LDS PA100E power amplifier. Simultaneously, two ends of the copper coil were clipped to the probe connected to DPO 4032 Oscilloscope to collect voltage response.

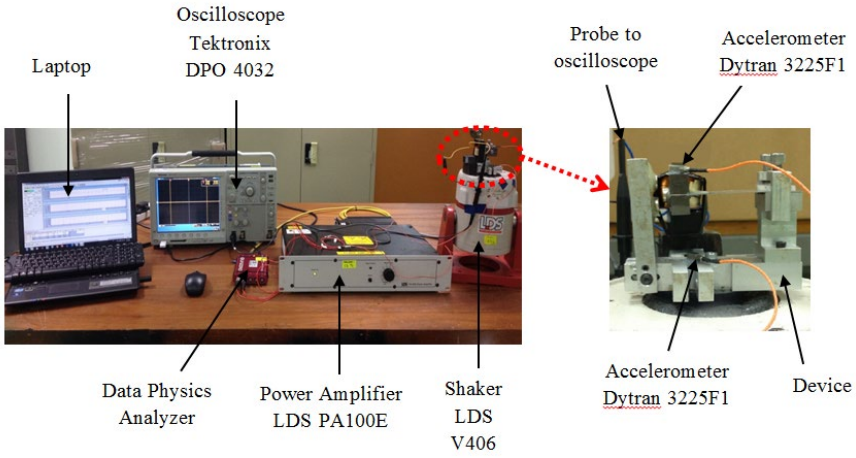

Figure 7. Experimental setup for dynamic measurement arrangement.

RESULTS AND DISCUSSION

Degree of non-linearity

The force-deflection relation of the system shown in Figure 2 can be represented by:

$$f = (k_b + k_{m1})z - k_{m3}z^3 \tag{13}$$

Here, the overall linear stiffness in Eq. (1), i.e. k_1 is composed of the fixed linear stiffness from the beam, k_b and the linear part of the magnetic stiffness, k_{m1}. The non-linear stiffness of the system, k_3 on the other hand, is contributed solely by the non-linear part of the magnetic stiffness, k_{m3}. Both linear and non-linear magnetic stiffnesses are dependent upon the gap, d between the magnets. The linear part of the magnetic stiffness, k_{m1} is proportional to $1/d^5$ while the non-linear part of the magnetic stiffness, k_{m3} is proportional to $1/d^7$ [5].

The relation between force and displacement is presented in Figure 8 for both linear and non-linear configurations. The solid black line in the graph represents a linear relation from the static equilibrium position to the maximum displacement. This is in line with the Hooke's law which governs linear configuration. Here, the stiffness of the system is wholly contributed by the linear stiffness of the beam since there is no magnet to change to the stiffness.

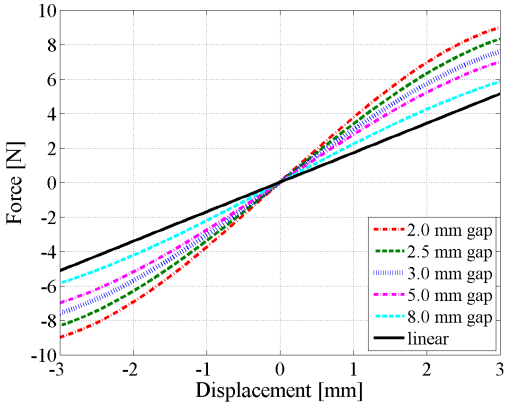

Figure 8. Force-displacement plot for linear configuration and non-linear configuration with different magnet gaps, *d*.

In the non-linear configuration, it is observed that the beam no longer abides by the linear Hooke's law as the correlation between force and displacement deviates from the direct proportionality relation as displacement increases. The trend of the force-displacement curves shown in Figure 8 for 2.0 mm, 2.5 mm, 3.0 mm, 5.0 mm and 8.0 mm magnet gaps are observed to only possess linear characteristic near the static equilibrium position. Notice that, the gradient of the force-displacement curve around the equilibrium position increases at the gap gets smaller. This is due to the addition of the linear magnetic stiffness, k_{m1} to the overall linear stiffness, k_1. For small displacement, the non-linear magnetic stiffness, k_{m3} is small due to the dependency on the cubic displacement. As the displacement increases, the linear proportionality no longer holds. The non-linear part of the magnetic stiffness, k_{m3} is now dominant over the linear stiffness giving rise to the softening behaviour. The dominancy of k_{m3} is more pronounced when the gap gets smaller, thus increases the strength of the non-linearity of the system.

The force and displacement data retrieved experimentally is used to calculate the degree of non-linearity for the respective non-linear configuration. The degree of non-linearity, α, was calculated using the expression obtained from the derivation of the non-dimensional equation of motion in Eq. (2) and this is given by

$$\alpha = \frac{k_3}{k_1} Y^2 \tag{14}$$

where k_3 is the non-linear stiffness, k_1 is the linear stiffness and Y is the amplitude of the input displacement. The values of k_1 and k_3 were retrieved from Figure 8 using the curve fitting method. Every curve shown in Figure 8 is curve fitted with a cubic polynomial function within the measured displacement range.

Table 2 summarises the values of k_1, k_3 and the calculated values of the non-linearity, α for all configurations. The negative sign for values of k_3 represents the non-linear softening characteristic resulting from the repulsive magnetic force. The more negative the value is, the stronger the degree of softening non-linearity. It is apparent from Table 2 that the non-linearity decreases when the gap of magnet increases. The decrement in the non-linearity suggests consistency with the force-displacement plot, where the characteristic of the non-linear configuration gradually converges to linear due to the weak contribution from the magnetic force as the gap becomes larger.

Table 2. Curve-fitted values of linear and non-linear stiffness with calculated non-linearity for $Y = 1.0$ mm.

Magnet gap, d (mm)	k_1 (Nmm^{-1})	k_3 (Nmm^{-3})	non-linearity, α
2.0	3.85	- 0.0952	$- 24.70 \times 10^{-3}$
2.5	3.46	- 0.0768	$- 22.18 \times 10^{-3}$
3.0	3.12	- 0.0653	$- 20.95 \times 10^{-3}$
5.0	2.82	- 0.0541	$- 19.17 \times 10^{-3}$
8.0	2.25	- 0.0337	$- 14.95 \times 10^{-3}$
linear	1.71	-	-

Frequency Response Curves

Linear configuration

Figure 9 shows the frequency response curve for the linear configuration. The peak resonance of this particular system is found at 20 Hz. The solid line represented by the frequency response curve only consists of single stable solutions where each response solely corresponds to each excitation frequency.

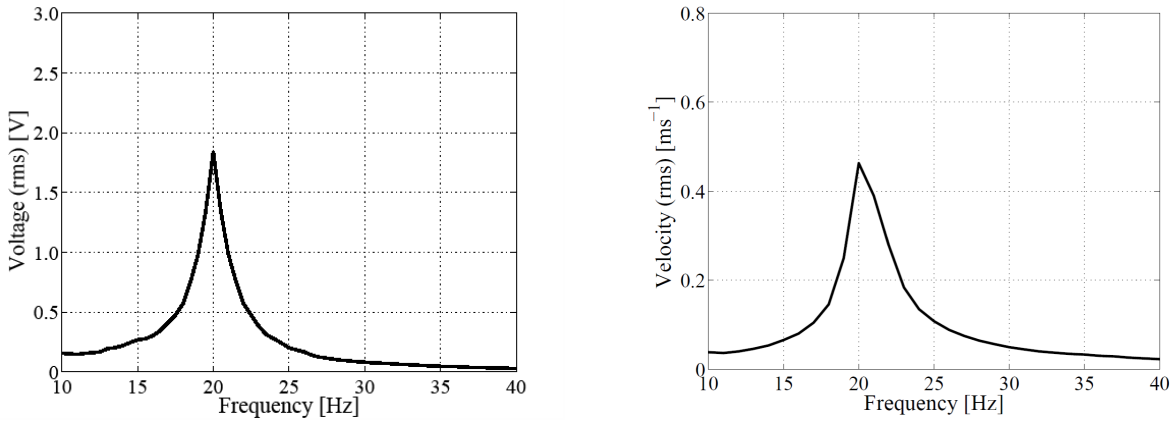

(a) (b)

Figure 9. (a) Voltage – frequency and (b) velocity – frequency plots for linear configuration.

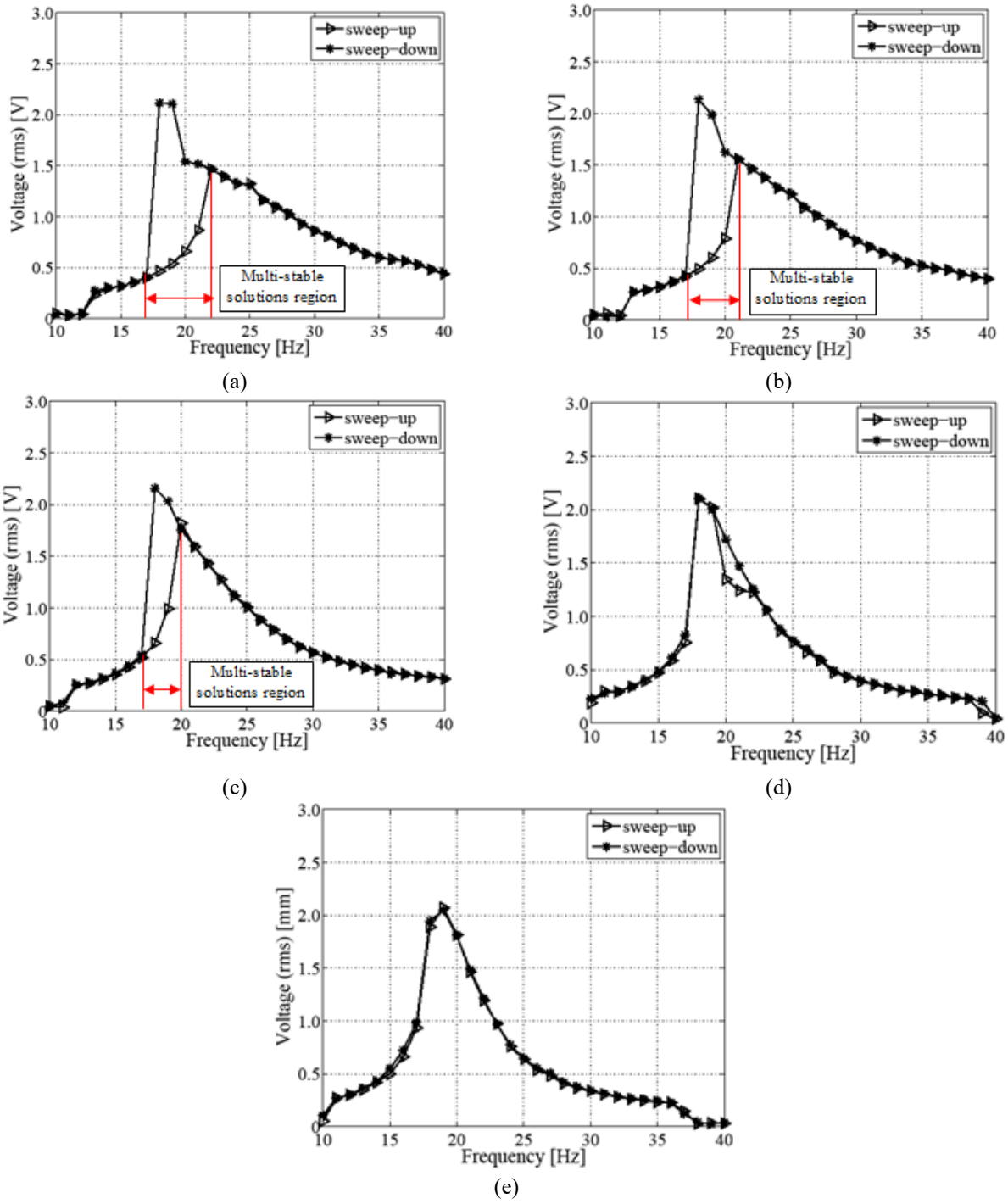

Figure 10. Voltage – frequency plot of non-linear configuration with different magnet gaps, *d*: (a) 2.0 mm, (b) 2.5 mm, (c) 3.0 mm, (d) 5.0 mm and (e) 8.0 mm.

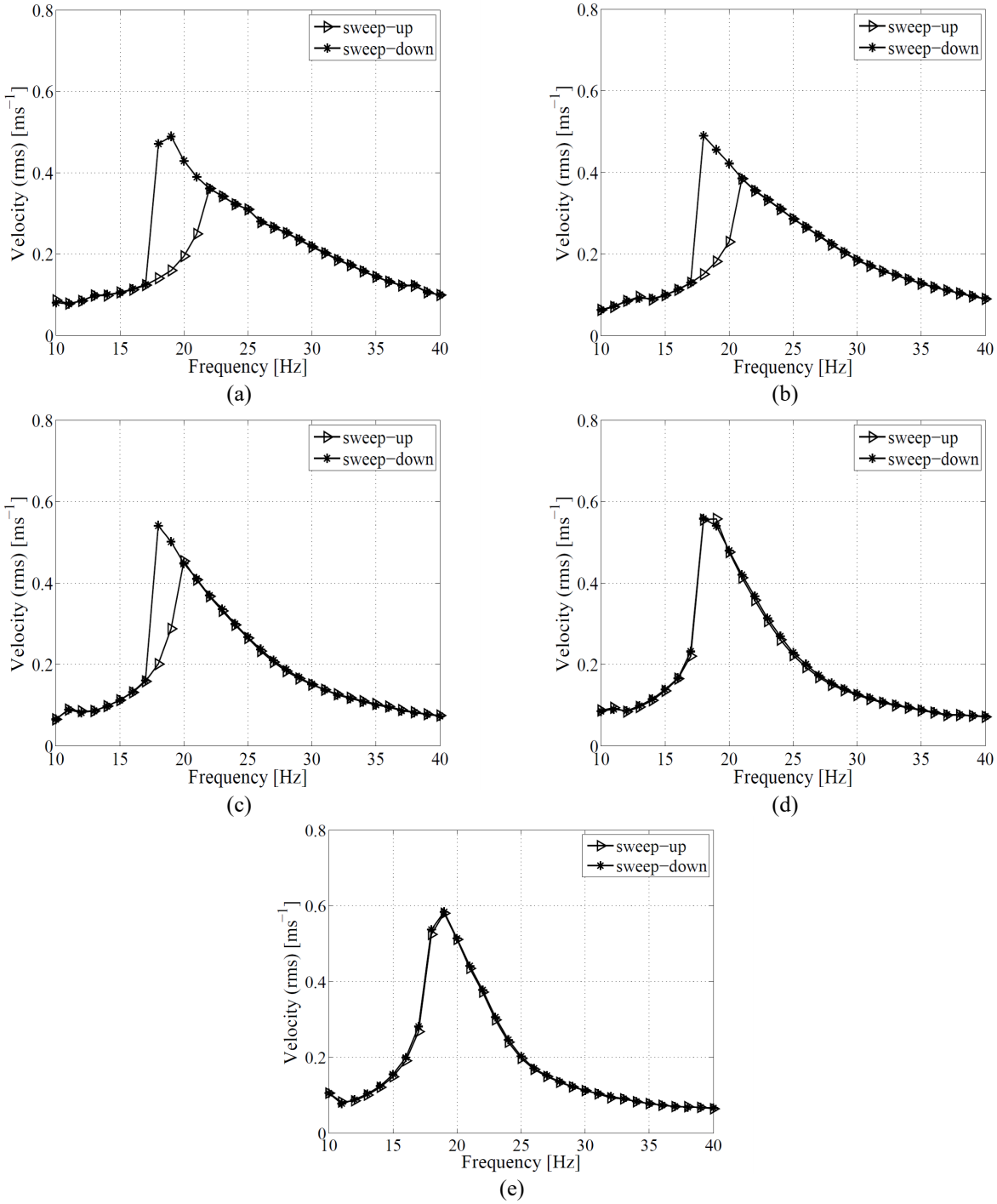

Figure 11. Relative velocity-frequency plot of non-linear configuration with different magnet gaps, *d:* (a) 2.0 mm, (b) 2.5 mm, (c) 3.0 mm, (d) 5.0 mm and (e) 8.0 mm.

Non-linear configuration

Frequency response curves for non-linear configuration are presented respectively in Figure 10 and 11 for different magnet gaps. There is a clear trend of the response curves bending to the left since the non-linearity of the device was affected by the softening effect as depicted in Figure 4. Analysing through Figure 10(a) to 10(c) for respective 2.0 mm, 2.5 mm and 3.0 mm gaps, the maximum response of the system appeared at 18 Hz. The multi-stable solutions region can be observed between the jump frequencies due to hysteresis. The strength of the non-linearity is also represented by the frequency range separating the jump-up and the jump-down point. A strong non-linear system has a large separation region. It can be seen from the figure that as the magnet gap increases, the separation region decreases. This is due to the decrease in the degree of the non-linearity as the gap increases, as presented previously in Table 2.

For magnet gap of 5.0 mm and 8.0 mm presented in Figure 10(d) and 10(e), it reveals that the characteristics of the frequency response curve has converged to the one shown in the linear configuration. Jump frequencies and multi-stable solutions region have not existed in these two weak non-linear systems. Equation (5) implies that for a weak non-linearity, α, the jump-down frequency approaches the linear natural frequency of the system, $\Omega_{\text{down}} \approx 1$, i.e. 20 Hz. The

convergence of the non-linear system can also be seen in Figure 5 as the non-linearity weakens. The sweep-up and sweep-down responses follow the same path indicating weak hysteresis even the stiffness of the system is still composed of both linear stiffness, k_1 and non-linear stiffness, k_3 as presented in Table 2.

The Transduction Coefficient

The device discussed in this paper represents the transformation of kinetic energy resulting from the beam oscillations to the voltage generated across the coil. Particularly, the relation between mechanical and electrical domain is quantified from the voltage generated, V to the relative velocity, v between the seismic mass and the coil in terms of transduction coefficient K which is expressed as Eq. (15) in Vsm^{-1}.

$$K = \frac{V}{v} \tag{15}$$

In this study, the transduction coefficient was not determined using the relation of $K = F/i$ where F is the restoring force at the tip of the beam, and i is a known value of DC current as performed in [17]. For the non-linear system, a sufficiently high value of DC current would need to be supplied in order to capture the non-linearity relation of the system. This is because the linear disproportionality is most apparent at larger displacement as depicted in Figure 8.

Linear configuration

Figure 12 presents the transduction coefficient – frequency plot for linear configuration. Considering that the transduction coefficient, K was taken as the ratio between voltage, V generated in Figure 9(a) to the relative velocity, v in Figure 9(b), the characteristic of the transduction coefficient plot is predicted to be constant across the frequency range. The constant transduction coefficient is due to the fixed rate of energy conversion from mechanical to the electrical domain. Thus, the proportionality for linearity is assumed to maintain across the frequencies.

The linear transduction coefficient is noticed between 15 Hz to 30 Hz while at low (10 Hz to 14 Hz) and high (31 Hz to 40 Hz) frequencies, the values of the transduction coefficient decrease. The small value of K at low frequencies is presumed to be subjected to the poor coherence between the input and output relation as well as the zero phase difference between the excitation and the response. Whereas at high frequencies, it was due to the high mechanical impedance that restricted the movement of the mass.

In this study, the low values of K at low and high frequencies are neglected because the region where the maximum response appeared for linear configuration is at 20 Hz, as presented in Figure 8. What is interesting in the value of K is its highest value at 30 Hz, which may easily lead to claim that the maximum response is taking place at this frequency. This claim is invalid because the maximum power depends on both the transduction coefficient and maximum response as given in Eq. (12). Therefore, even when K is large at a particular frequency, it may not correspond to the maximum time-averaged power due to a small response. For current linear configuration, the transduction coefficient is indicated at 20 Hz, which is at the maximum response of the system.

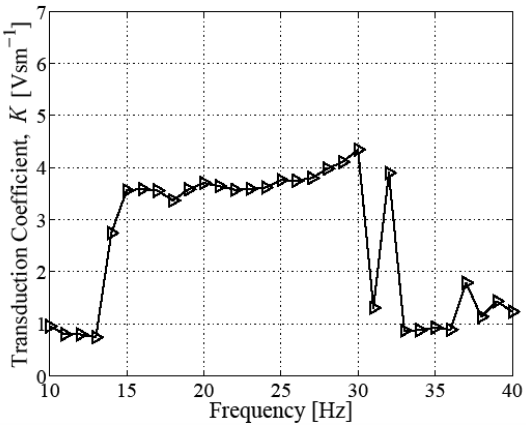

Figure 12. Transduction coefficient plot for linear configuration.

Non-linear configuration

In the frequency response curve results for the non-linear configuration earlier, it was shown that the multi-stable solutions region existed between the jump frequencies. For linear configuration, the transduction coefficient is noticed to be constant across the frequency range. Figure 13 presents the transduction coefficient – frequency plot for the non-linear configuration with different magnet gaps. The transduction coefficients are computed similarly to results in Figure 11, i.e. by taking the ratio of the generated voltage to the relative velocity. The most interesting aspect is noticed throughout Figure 13(a) to 13(c) with 2.0 mm, 2.5 mm and 3.0 mm configuration, respectively, where the linear proportionality of the transduction coefficient only hold at low and high frequency, outside the multi-stable solutions region. The value of K is determined to be at 18 Hz, where the maximum response was observed in the frequency response curves in Figure 9

and 10. Similar to the linear configuration, the low values of K at low frequencies was due to the poor coherence and zero phase difference. Also, the higher values of K (35 Hz to 40 Hz) which are higher than the K at the maximum response (18 Hz) are not being taken into consideration since the maximum response do not appear at high frequencies. A comparison of the linear and non-linear configuration reveals that the non-linear system produces larger transduction coefficient compared to its equivalent linear system, which produces almost constant transduction coefficient outside the multi-stable region. These results suggest that the mechanical and electrical part of the system couples better when the system is operating non-linearly.

Another significant aspect is found in Figure 13(d) and 13(e), where it was pointed out in the frequency response curves earlier that as the gap of magnet increases, the dynamic characteristic would converge to linear characteristic. Consistently, the transduction coefficient for 5.0 mm and 8.0 mm magnet gaps behave almost linearly. Although both are classified under the non-linear configuration, the non-linearity for these two magnet gaps are considered to be very weak as the jump frequencies, and multi-stable solutions region is not clearly visible as observed in Figure 10(d) and 10(e). In the region between 19 Hz to 22 Hz observed in Figure 10(d), it may appear that the multi-stable solutions existed. However, this is presumed not to be entirely true as the difference in K values is caused by the slight difference in the response from the sweep-up and sweep-down voltage generated based on the data collection.

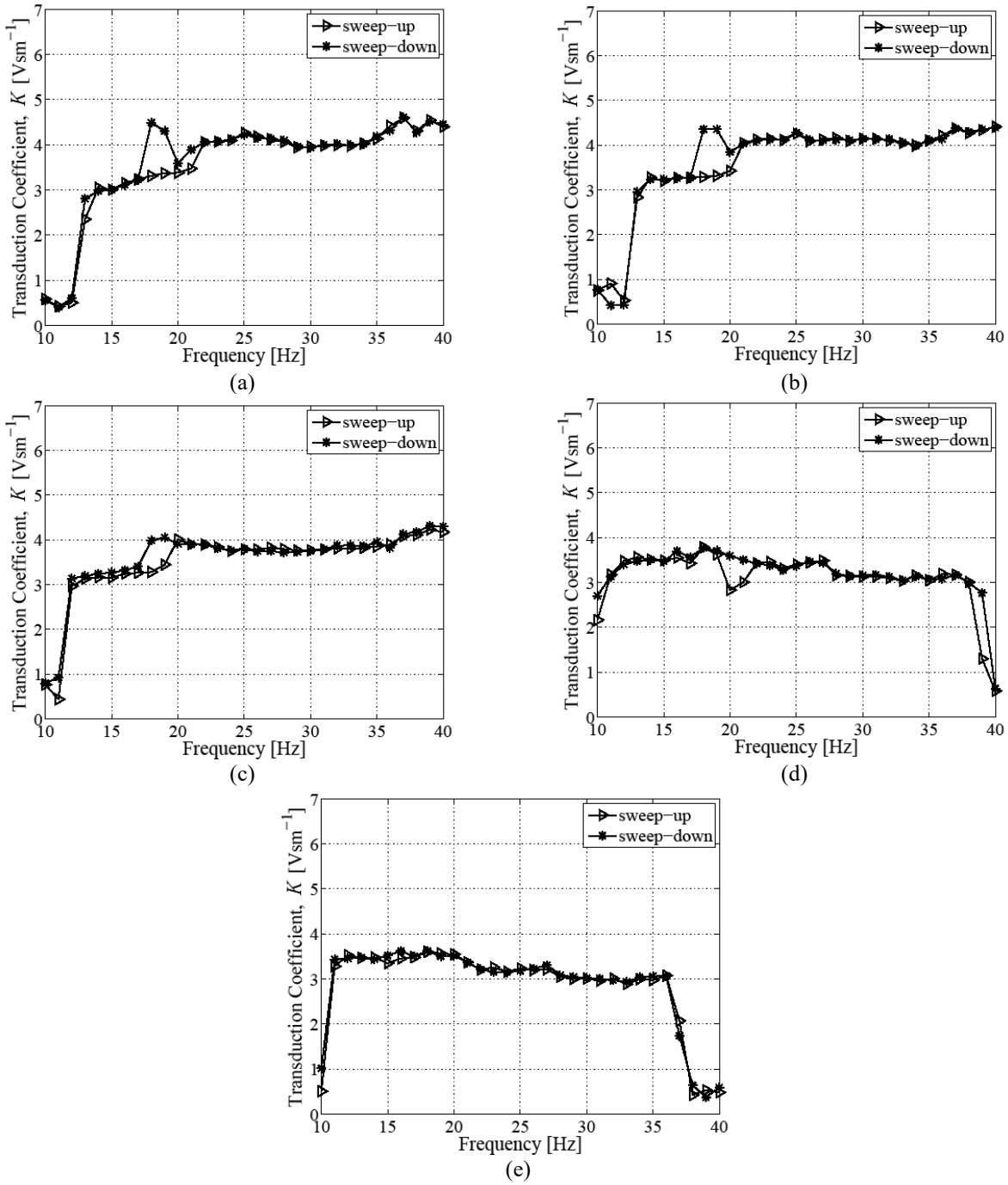

Figure 13. Transduction coefficient plot for non-linear configuration with (a) 2.0 mm, (b) 2.5 mm, (c) 3.0 mm, (d) 5.0 mm and (e) 8.0 mm gap of magnet.

The values of transduction coefficient, K retrieved at the maximum response for the linear, and non-linear configuration are summarised in Table 3. The values of K at the maximum response decrease with the increment of the gap of the magnet, which corresponds to the decrease in the non-linearity, α. The value of K converges to the one from the linear configuration when the non-linearity weakens as shown when the gap is 5 mm. An exception for is given for the value obtained for 8 mm gap, where the value reported in Table 3 may not represent the exact behaviour of the system due to fluctuation in the dynamic response. One of the reasons for the fluctuation is due to the inconstant level of input supplied by the shaker. During the conduct of the experiment, the level of input was controlled manually by controlling the gain so that the amplitude of input displacement was maintained at 1 mm. The control is even harder at points close to jump-down frequency.

Table 3. Summary of transduction coefficient for linear and non-linear configurations.

Magnet gap (mm)	Transduction coefficient, K (Vsm^{-1})
2	4.49
2.5	4.36
3	3.99
5	3.77
8	3.51
linear	3.71

So far, the transduction coefficient for both the linear and non-linear configurations has been determined at the maximum response. Unlike the linear configuration where the transduction coefficient is constant across the frequency range, the non-linear configuration opens up question on the validity of employing the linear transduction coefficient when estimating its power generation. Based on the results presented in Figure 13, the transduction coefficient for the non-linear system appeared to be larger than the linear counterpart at the maximum response where multi-stable solutions exist. Estimating the transduction coefficient using the ratio between the induced electromagnetic force and the applied DC current described in [17] may not represent the actual transduction coefficient of the non-linear system thus underestimating the amount of power that could be generated by the non-linear system. The following part of this paper moves on to examine the harmonic ratio of the respective configurations in order to determine the limit of using linear transduction coefficient in the non-linear system.

Harmonic Ratio

The harmonic ratio for both the linear and non-linear configurations were examined to determine the limit of employing linear transduction coefficient on the non-linear system. The harmonic ratio was analysed between the fundamental harmonic, ω with the second harmonic, 3ω in the form of percentage values. The 2ω harmonic is considered negligible as it was caused by the asymmetry from the gravity.

Linear configuration

Based on the harmonic ratio results presented in Figure 14, the lowest harmonic, ω (known as the fundamental harmonic) is produced when the system is subjected to sinusoidal excitation where input is equivalent to output in the linear system. The linear system is reported to be dominated by the fundamental harmonic as the percentage ratio of the second harmonic 3ω to the fundamental harmonic, ω across the frequency are of negligible percentage values.

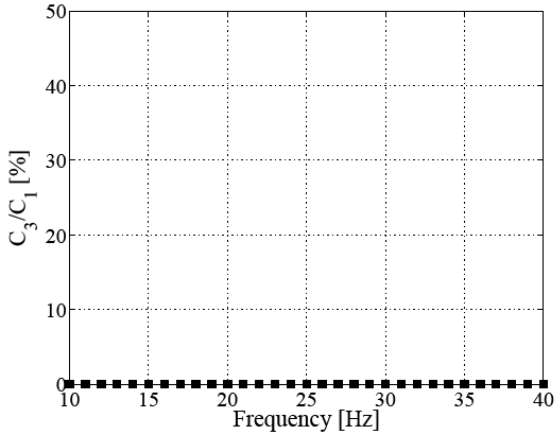

Figure 14. The harmonic ratio for linear configuration.

Non-linear configuration

Figure 15 displays the harmonic ratio for the non-linear configuration with different magnet gaps. For a non-linear system, where the input is not equivalent to the output, higher harmonics are predicted in the response of the system. Referring to the 2.0 mm magnet gap in Figure 15(a) with the highest non-linearity, the effect of the second harmonics is

evident from 18 Hz towards 40 Hz. When the maximum response jumps down to the non-resonant branch at 17 Hz, as observed in Figure 10(a), the second harmonic has appeared to be negligible. At the non-resonant branch with low frequency, the second harmonic is hardly produced because the device operates in the linear region as shown in Figure 8.

By analysing the maximum response at 18 Hz, the harmonic ratio decreases gradually towards the high-frequency range signifying the reduction of the second harmonic when frequency increases. At 26 Hz, where the peak of the harmonic ratio is relatively higher, it does not suggest that the second harmonic is the strongest at this particular frequency because the degree of non-linearity is not determined solely by the percentage of the harmonic ratio at this particular frequency. As for the high harmonic ratio noticeable at 10 Hz and 11 Hz, it also does not represent that the second harmonic is at its strongest. This inconsistency may be due to noise occurred at low frequencies and can be neglected as shown by the frequency response curve where only non-resonant branch exists.

Figure 15(b) shows the harmonic ratio for 2.5 mm magnet gap. Due to the decrease of non-linearity, the effect of the second harmonic has covered less across the frequency range from the maximum response frequency, which is from 18 Hz to only 35 Hz. This explains that the effect of the second harmonic has decreased as the non-linearity decreases. The relatively higher harmonic ratio observed between 18 Hz to 25 Hz compared to Figure 15(a) is thought to be caused by the difficulty in keeping the input displacement to be constant at the resonance region. Therefore, Figure 15(a) and 15(b) may not be suitable to be justified in terms of percentage in this case. Instead, both can be justified through the frequency range of the second harmonic effect.

By analysing the harmonic ratio results for 3.0 mm, 5.0 mm and 8.0 mm magnet gaps in Figure 15(c), 15(d) and 15(e) accordingly, significant reduction of the second harmonic is observed. In Figure 15(c) and 15(d), the effect of the second harmonic is only visible from the maximum response of 18 Hz to 26 Hz with the latter at a ratio less than 5% values. In Figure 15(e), the second harmonic ratio is visible at 18 Hz to 20 Hz and 25 Hz to 26 Hz, with ratio values of less than 5%. These findings suggest that with a further decrement of non-linearity as the magnet gap increases, the harmonic ratio decreases and gradually converges to the harmonic ratio shown for the linear configuration.

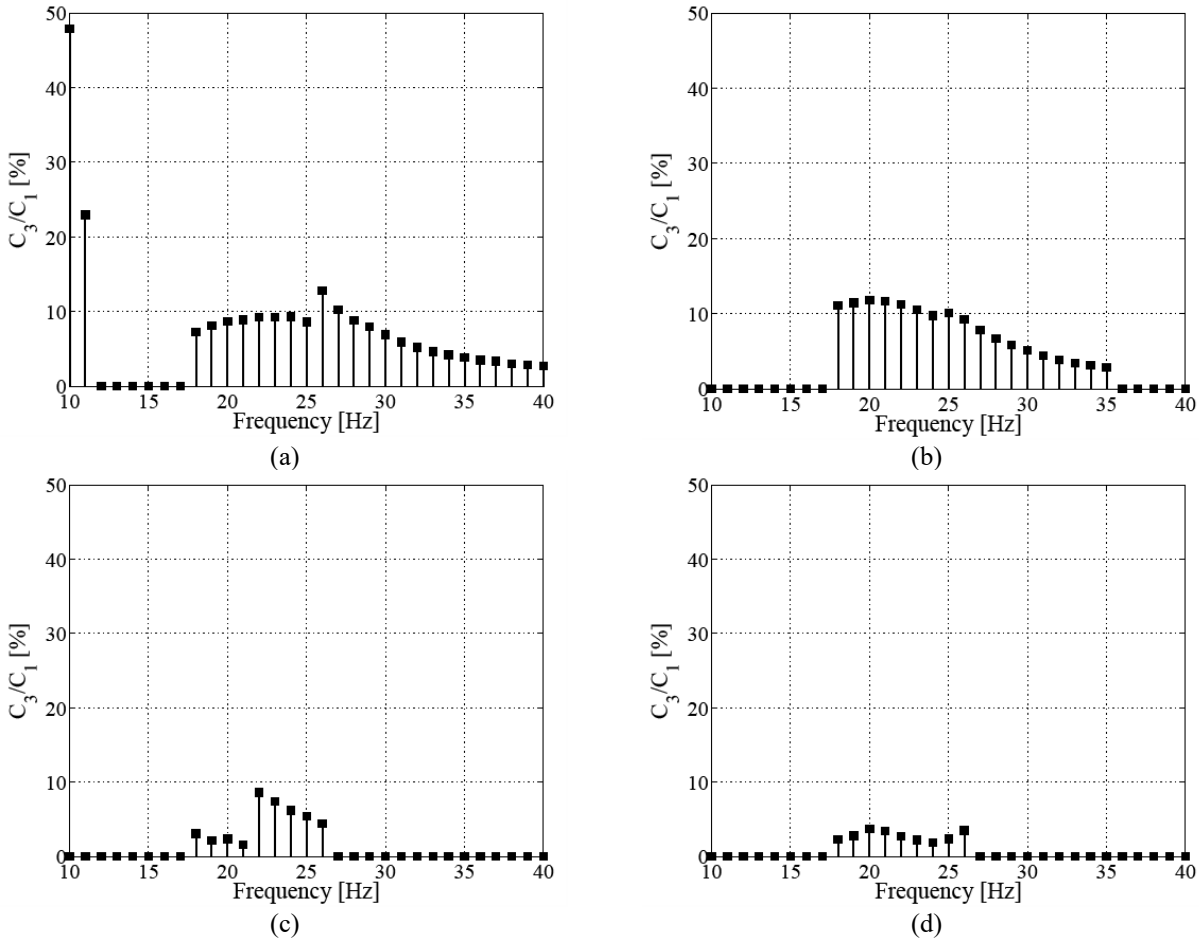

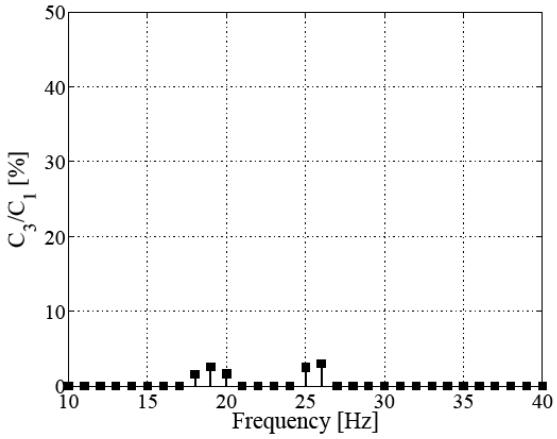

(e)

Figure 15. The harmonic ratio for non-linear configuration with (a) 2.0 mm, (b) 2.5 mm, (c) 3.0 mm, (d) 5.0 mm and (e) 8.0 mm gap of magnet.

The findings from the harmonic ratio results have important implications in setting the limit of using linear transduction coefficient on the non-linear system. Primarily, the limit can be determined according to the percentage of harmonics at the multi-stable solutions region. When the harmonic ratio is less than five per cent (< 5%) at the multi-stable solutions region where the maximum response occurred, the non-linear system is concluded as weak. If the harmonic ratio is more than 5% in the non-linear system, the usage of linear transduction coefficient may not be accurate as it does not represent the strong effect of second harmonics and the actual transduction at the multi-stable solutions region. Thus, the assumption of employing linear transduction coefficient in the non-linear system as suggested in the literature review may underestimate the actual amount of power that can be harvested by a system with non-linear stiffness.

CONCLUSION

The present study was designed to investigate the transduction coefficient for the linear and non-linear system across the frequency range of interest. Transduction coefficient of a non-linear system energy harvesting device has not been given suitable attention since the benefit of the stiffness non-linearity in an energy harvesting device has been solely awarded to the bandwidth widening. This study reveals that the transduction coefficient for the presented non-linear configuration is larger compared to the equivalent linear system in the region of multi-stable solutions, where the maximum response of the system is recorded.

This paper also reveals experimentally that the degree of non-linearity decreases as the magnet gap increases in the non-linear configuration and gradually converges to the characteristic of the linear system. Likewise, the transduction coefficient for the non-linear system gradually decreases as the degree of non-linearity decrease and at one point, converges to the linear transduction coefficient. In order to draw the limit of using the linear transduction coefficient on the non-linear system, the harmonic ratio for the non-linear configuration was studied, and the limit was set based on the percentage of higher harmonics at the multi-stable solutions region. The assumption of employing linear transduction coefficient on the non-linear configuration turns to be less accurate when the percentage of higher harmonics were less than five per cent at the multi-stable solutions region.

ACKNOWLEDGEMENT

The authors would like to acknowledge the financial support from the Ministry of Higher Education Malaysia and the Universiti Teknikal Malaysia Melaka through the Fundamental Research Grant Scheme (FRGS/2/2013/TK01/FKM/02/2/F00172).

REFERENCES

[1] Chunfang L, Shuai W, Patrick CKL, Min G, Zongxia J. Enhanced bandwidth non-linear resonance electromagnetic human motion energy harvester using magnetic-springs and ferrofluid. IEEE/ASME Transactions on Mechatronics 2019; 24(2): 710-717.

[2] Zhongxin Y, Weiqun L, Shuang Z, Qiao Z, Guangdi H. Bandwidth broadening through stiffness merging using the non-linear cantilever generator. Mechanical Systems and Signal Processing 2019; 132: 1-17.

[3] Kangqi F, Yiwei Z, Haiyan L, Meiling C, Qinxue T. A non-linear two-degree-of-freedom electromagnetic energy harvester for ultra-low frequency vibrations and human body motions. Renewable Energy 2019; 138: 292-302.

[4] Talib NHHA, Salleh H, Youn BD, Resali MSM. Comprehensive review on effective strategies and key factors for high performance piezoelectric energy harvester at low frequency. International Journal of Automotive and Mechanical Engineering, 2019; 16(4): 7181 – 7210.

[5] Tang L, Yang Y, Soh, C-K. Improving functionality of vibration energy harvesters using magnets. Journal of Intelligent Material Systems and Structures, 2012; *23*(13), 1433 – 1449.

[6] Berdy DF, Valentin DJ, Peroulis D. Kinetic energy harvesting from human walking and running using a magnetic levitation energy harvester. Sensors and Actuators A 2015; 222**:** 262 – 271.

[7] Bouendeu E, Greiner A, Smith PJ, Korvink JG. An efficient low cost electromagnetic vibration harvester. In: Proceedings of Power MEMS, Washington DC, USA, pp. 320 –23; 2009.

[8] Büren T, Tröster G. Design and optimisation of a linear vibration-driven electromagnetic micro-power generator. Sensors and Actuators A 2007; 135(2): 765–75.

[9] Foisal ARM, Chung GS. Fabrication and characterisation of a low frequency electromagnetic energy harvester. Journal of Semiconductors 2012; 33(7): 074001(1)-(5).

[10] Galchev T, McCullagh J, Peterson RL, Najafi K. A vibration harvesting system for bridge health monitoring applications. In: Proceedings of Power MEMS, Leuven, Belgium, pp. 3–6; 2010.

[11] Kulkarni S, Koukharenko E, Torah R, Tudor J, Beeby S, O'Donnell T, Roy S. Design, fabrication and test of integrated micro-scale vibration-based electromagnetic generator. Sensors and Actuators A 2008; 145-146: 336–42.

[12] Lee BC, Rahman MA, Hyun SH, Chung GS. Low frequency driven electromagnetic energy harvester for self-powered system. Smart Materials Structures 2012; 21(12): 125024-30.

[13] Vishwas B, Josiah O, Shashank P. Pen harvester for powering a pulse rate sensor. Journal of Physics D 2009; 42(10): 105105-13.

[14] Kazmierski T, Beeby S. Energy harvesting systems: principles, modeling and applications. New York: Springer; 2011.

[15] Constantinou P, Mellor PH, Wilcox PD. A magnetically sprung generator for energy harvesting applications. IEEE/ASME Transactions on Mechatronics 2012; 17(3): 415–24.

[16] Mann BP, Sims ND. Energy harvesting from the non-linear oscillations of magnetic levitation. Journal of Sound and Vibration 2009; 319: 515–530.

[17] Cheng S, Wang N, Arnold DP. Modeling of magnetic vibrational energy harvesters using equivalent circuit representations. Journal of Micromechanics and Microengineering 2007; 17(11): 2328–2335.

[18] Baker E, Reissman T, Zhou F, Wang C, Lynch K, Sun C. Microstereolithography of three-dimensional polymeric springs for vibration energy harvesting. Smart Materials Research 2012; 1–9.

[19] Rossi M. Acoustics and Electroacoustics. Norwood, United States: Artech House; 1988.

[20] Challa VR, Cheng S, Arnold DP. The role of coupling strength in the performance of electrodynamic vibrational energy harvesters. Smart Materials and Structures 2012; 22(2): 025005-025015.

[21] Cheng S, Natarajan RD, Arnold DP. The importance of coupling strength for maximising the output power of electrodynamic vibrational energy harvesters. In: Proceedings of Power MEMS, Leuven, Belgium, pp. 351–354; 2010.

[22] Liu H, Gudla S, Hassani FA, Heng CH, Lian Y, Lee C. Investigation of the non-linear electromagnetic energy harvesters from hand shaking. IEEE Sensors Journal 2015; 15(4): 2356 – 2364.

[23] Ramlan R, Brennan MJ, Mace BR, Kovacic I. Potential benefits of a non-linear stiffness in an energy harvesting device. non-linear Dynamics 2010; 59: 545 – 558.

[24] Stephen NG. On energy harvesting from ambient vibration. Journal of Sound and Vibration 2006; 293(1–2): 409-425.

[25] Barton DAW, Burrow SG, Clare LR. Energy harvesting from vibrations with a non-linear oscillator. Journal of Vibration and Acoustics 2010; 132(2): 021009 1 - 15.